

Article

Simulation and Study of DC Corona Discharge Characteristics of Bar-Plate Gap

Na Feng ^{1,2,*} , Tiehua Ma ^{1,2}, Changxin Chen ^{1,2}, Boren Yao ^{1,2} and Weitao Gao ^{1,2}

¹ State Key Laboratory of Dynamic Measurement Technology, North University of China, Taiyuan 030051, China

² School of Electrical and Control Engineering, North University of China, Taiyuan 030051, China

* Correspondence: fengna@st.nuc.edu.cn

Abstract: In this paper, the corona discharge process of the bar-plate gap at -1 kV DC voltage is simulated using a two-dimensional axisymmetric plasma module. We analyze the variation of air negative corona discharge current, and the distribution morphology of microparticles in different discharge stages in detail. The significance of plasma chemical reactions at some typical time and the distribution characteristics of heavy particles are investigated according to reaction rates. Results show that, in the current rising stage, the collision ionization reactions (e.g., R_1 and R_2) and electron adsorption reaction (e.g., R_3) play a major role, which lead to the increase in charged particles and the formation of an electron avalanche. In the current drop stage, all reaction rates decreased, except for collision ionization and electron attachment, partial charge transfer reactions (e.g., R_8 , R_{10} , R_{11} , and R_{14}), and composite reactions (e.g., R_{16} , R_{17} , and R_{18}), which come into play and gradually reduce the number of charged ions in the gap. In the current stabilizing stage, the main chemical reactions are composite reactions (e.g., R_{16} and R_{17}), then the corona discharge ends. For the heavy particle distribution, O_2^+ and O_4^+ are the main positive ions, O_2^- is the most abundant negative ions, and the neutral particles are mainly O.

Keywords: DC negative corona; air; bar-plate gap; plasma model; discharge morphology; heavy particles distribution



Citation: Feng, N.; Ma, T.; Chen, C.; Yao, B.; Gao, W. Simulation and Study of DC Corona Discharge Characteristics of Bar-Plate Gap. *Energies* **2022**, *15*, 6431. <https://doi.org/10.3390/en15176431>

Academic Editors: Richard Cselko and Bálint Németh

Received: 4 August 2022

Accepted: 30 August 2022

Published: 2 September 2022

Publisher's Note: MDPI stays neutral with regard to jurisdictional claims in published maps and institutional affiliations.



Copyright: © 2022 by the authors. Licensee MDPI, Basel, Switzerland. This article is an open access article distributed under the terms and conditions of the Creative Commons Attribution (CC BY) license (<https://creativecommons.org/licenses/by/4.0/>).

1. Introduction

Corona discharge is a partial discharge phenomenon occurring near the electrode with a small radius of curvature in an uneven electric field. When the electric field intensity exceeds the ionization field intensity, the air gap will be broken down, accompanied by electrical, acoustic, and optical phenomena [1]. The corona discharge will have an irreversible impact on the power system. First, the physical reactions in the discharge process will cause energy loss. Second, the appearance of corona will increase the gas temperature around the transmission equipment and reduce the thermal stability of the transmission equipment. Finally, in the radius of curvature at smaller places, the microparticles are accelerated by a strong field, and the electrode is subjected to force vibration and torsion, which will reduce the dynamic stability of the power transmission equipment. Therefore, the study of corona discharge characteristics has crucial practical significance [2–4].

In the microscopic process of corona discharge, various particles (such as ions, free radicals, and excited particles) will be produced, leading to further complex physical and chemical reactions. In early research, people simulated the gas discharge process by establishing a circuit model [5]. However, the plasma discharge process lacks an effective measurement method. Then, scientists began to choose the numerical simulation method to conduct in-depth research on the micro process of corona discharge [6,7].

The numerical simulation method can be used to obtain the variation of space/surface charge and local field distribution with time in the corona discharge process and realize

the quantitative analysis of the interaction between charge distribution and discharge process [8]. In addition, numerical simulation can compensate for the deficiency of actual measurement when studying the micro-physical mechanism of the discharge process.

In the research of using a simulation model to analyze corona discharge characteristics, Chen et al. [9] built a three-species corona model coupled with gas dynamics in COMSOL Multiphysics, and calculated the mean current, Trichel pulse frequency and flow velocity. The ionic wind mechanism in the Trichel pulse stage was revealed. Gao et al. [10] used the fluid dynamic drift–diffusion theory of finite element simulation software COMSOL to simulate SF₆ gas negative corona discharge and obtained the space–time characteristics of the SF₆ gas Trichel pulse. They measured the distribution of charged particles and the total number of charged particles with time. In Reference [11], the characteristics of heavy particles in bar-plate DC positive corona discharge were studied. An improved, multicomponent, and 2D hybrid model was used in the simulation. The electric field distribution and net space charge distribution at typical times, and the composition and distribution of particles were analyzed. Peng et al. [12] built a global model of atmospheric pressure humid air discharge plasma and researched the variation of charged particles densities and chemical reaction rates with time. The key particles and chemical reactions reflecting the chemical process of atmospheric pressure discharge plasma in humid air were summarized. Based on the hydrodynamic model and the collision reaction model, Liao et al. [13] improved the bar-plate electrode negative corona discharge model. They analyzed the time–space development laws of electric field intensity, plasma chemical reaction rate, space charge density, and electron density distribution in the process of Trichel pulse. He et al. [14] researched the negative corona discharge pulse characteristics of the needle electrode structure of SF₆/N₂ gas mixture under DC voltage. They analyzed the effects of air pressure, gap distance, and content of N₂ on the initial voltage and pulse characteristic parameters. The results showed that the current pulse is mainly distributed irregularly with a small amplitude. To sum up, there are few reports on the plasma equations and heavy particle microscopic characteristics of DC negative corona bar-plate gap discharge.

This paper proposes a plasma simulation model based on the hydrodynamic model. The plasma chemistry model is established on the simulation software COMSOL Multiphysics, and the variation curve of the discharge current in the discharge channel is obtained. The distribution morphologies of the electric field intensity E , space charge density ρ , electron number density N_e , positive ion number density N_p , and negative ion number density N_n are analyzed at the typical times. Subsequently, this work summarizes the main chemical reactions in the plasma model according to the reaction rates and the distribution law of heavy particles at different times and analyzes the air negative corona discharge characteristics from the perspective of microparticles. The rest of this paper is arranged as follows. The corona discharge model of bar-plate gap is established in Section 2. The process of DC negative corona discharge is analyzed according to the pulse current curve and corona discharge topography in Section 3. Section 4 presents the importance of plasma chemical reactions and the distribution of heavy particles in air corona discharge. Finally, the conclusion is given in Section 5.

2. Corona Discharge Model of Bar-Plate Gap

2.1. Hydrodynamic Governing Equation

The hydrodynamic numerical simulation model is a commonly used model in the corona pulse simulation research, which mainly includes the continuity equation and Poisson equation [15]. To describe the microscopic physical process of corona discharge, the plasma chemical reaction model is added in this paper, and some additional terms are added based on the traditional governing equation.

We obtained the number density of charged particles by solving continuity Equations (1)–(3) and coupling with Poisson Equations (4) and (5). The number density of

charged particles can reflect the movement of charged particles in the bar-plate gap, that is the generation and disappearance of particles [8,16,17]:

$$\frac{\partial n_e}{\partial t} + \nabla \left(-n_e \mu_e \vec{E} - D_e \nabla n_e \right) = \alpha n_e \left| \mu_e \vec{E} \right| - \eta n_e \left| \mu_e \vec{E} \right| - k_{ep} n_e n_p, \tag{1}$$

$$\frac{\partial n_p}{\partial t} + \nabla \left(n_p \mu_p \vec{E} - D_p \nabla n_p \right) = \alpha n_e \left| \mu_e \vec{E} \right| - k_{ep} n_e n_p, \tag{2}$$

$$\frac{\partial n_n}{\partial t} + \nabla \left(-n_n \mu_n \vec{E} - D_n \nabla n_n \right) = \eta n_e \left| \mu_e \vec{E} \right| - k_{np} n_n n_p, \tag{3}$$

$$\epsilon_0 \epsilon_r \nabla^2 \phi = -q (n_p - n_n - n_e), \tag{4}$$

$$\vec{E} = -\nabla \phi, \tag{5}$$

where n_e , n_p and n_n are the number densities of electrons, positive ions and negative ions, $1/m^3$; μ_e , μ_p , μ_n , D_e , D_p , and D_n are mobilities (m^2/Vs) and diffusion coefficients (m^2/s) of electrons, positive ions, and negative ions, respectively; \vec{E} is the electric field vector, V/m ; α is ionization coefficient, $1/m$; η is the attachment coefficient, $1/m$; k_{ep} is the recombination coefficients of electrons and positive ions, m^3/s ; k_{np} is the recombination coefficients of negative and positive ions, m^3/s ; ϵ_0 is the vacuum permittivity, F/m ; ϵ_r is the relative permittivity, F/m ; and ϕ is the potential, V .

In the above governing equations, the setting of each parameter has a direct influence on the final calculation result of a negative corona discharge. The air discharge parameters used in this paper are from the experimental parameters provided by Nikonov [18].

During corona discharge, electrons migrate and diffuse because of the action of the electric field force, and the electron number density in the gap changes correspondingly. The mobility and diffusion coefficient of electrons are differed from those of positive and negative ions, so the charge distribution in the gap will change.

2.2. Air Electrochemical Reaction Process

In this paper, the air plasma chemical reaction process mainly contains 12 particles, namely, e , N_2^+ , N_2 , O_2 , O_2^- , O , O^- , O_4^+ , N_4^+ , O_2^+ , $N_2O_2^+$, and O_3 . The specific reaction process and relevant data [7,19,20] are shown in Table 1.

Table 1. Air plasma gas-phase reactions.

No.	Reaction Process	Rate Coefficient ¹	ΔE ²
R ₁	$N_2 + e \Rightarrow 2e + N_2^+$	$f(\epsilon)$	15.6
R ₂	$O_2 + e \Rightarrow 2e + O_2^+$	$F(\epsilon)$	12.1
R ₃	$2O_2 + e \Rightarrow O_2 + O_2^-$	$6.0 \times 10^{-39} T_e^{-1}$	
R ₄	$O_4^+ + e \Rightarrow 2O_2$	$2.42 \times 10^{-11} T_e^{-0.5}$	
R ₅	$O_2^+ + e \Rightarrow 2O$	$6.0 \times 10^{-11} T_e^{-1}$	
R ₆	$N_2^+ + N_2 + O_2 \Rightarrow N_4^+ + O_2$	5.0×10^{-41}	
R ₇	$N_2^+ + N_2 + N_2 \Rightarrow N_4^+ + N_2$	5.0×10^{-41}	
R ₈	$N_4^+ + O_2 \Rightarrow O_2^+ + 2N_2$	2.5×10^{-16}	
R ₉	$N_2^+ + O_2 \Rightarrow O_2^+ + N_2$	$1.04 \times 10^{-15} T^{-0.5}$	
R ₁₀	$2N_2 + O_2^+ \Rightarrow N_2O_2^+ + N_2$	$8.1 \times 10^{-38} T^{-2}$	
R ₁₁	$N_2O_2^+ + N_2 \Rightarrow O_2^+ + 2N_2$	$14.8 T^{-5.3} \exp(-2357/T)$	
R ₁₂	$N_2O_2^+ + O_2 \Rightarrow O_4^+ + N_2$	1.0×10^{-15}	
R ₁₃	$O_2^+ + O_2 + O_2 \Rightarrow O_4^+ + O_2$	$2.04 \times 10^{-34} T^{-3.2}$	
R ₁₄	$O_2^+ + O_2 + N_2 \Rightarrow O_4^+ + N_2$	$2.04 \times 10^{-34} T^{-3.2}$	
R ₁₅	$O_4^+ + O_2^- \Rightarrow 3O_2$	1.0×10^{-13}	
R ₁₆	$O_4^+ + O_2^- + O_2 \Rightarrow 3O_2 + O_2$	2.0×10^{-37}	
R ₁₇	$O_4^+ + O_2^- + N_2 \Rightarrow 3O_2 + N_2$	2.0×10^{-37}	
R ₁₈	$O_2^+ + O_2^- + O_2 \Rightarrow 2O_2 + O_2$	2.0×10^{-37}	
R ₁₉	$O_2^+ + O_2^- + N_2 \Rightarrow 2O_2 + N_2$	2.0×10^{-37}	
R ₂₀	$O + O_2 + O_2 \Rightarrow O_3 + O_2$	2.5×10^{-46}	
R ₂₁	$O + O_2 + N_2 \Rightarrow O_3 + N_2$	2.5×10^{-46}	
R ₂₂	$e + N_2^+ + N_2 \Rightarrow 2N_2$	$6.07 \times 10^{-34} T_e^{-2.5}$	
R ₂₃	$N_2^+ + 2e \Rightarrow N_2 + e$	$5.651 \times 10^{-27} T_e^{-0.8}$	

¹ The units of two-body reaction-rates are m^3/s , three-body reaction-rates are m^6/s ; T is environment temperature, T_e is electronic temperature, K. ² ΔE is the energy loss during electron collision, eV.

All surface reactions in the plasma model are shown in Table 2. Charged and unstable neutral particles are assumed to return to the plasma where parent neutral molecules exist. The adhesion coefficient represents the influence of all excited neutral particles, free radicals, and ion types on the surface reactions.

Table 2. Air plasma surface reactions.

No.	Surface Reaction Process	Adhesion Coefficient
S ₁	$O_2^+ \Rightarrow O_2$	1
S ₂	$N_2^+ \Rightarrow N_2$	1
S ₃	$N_4^+ \Rightarrow 2N_2$	1
S ₄	$N_2O_2^+ \Rightarrow 2N_2 + O^2$	1
S ₅	$O_4^+ \Rightarrow 2O_2$	1
S ₆	$O_2^- \Rightarrow O_2$	1
S ₇	$O^- \Rightarrow 0.5O_2$	1
S ₈	$O \Rightarrow 0.5O_2$	1

2.3. Boundary Conditions and Algorithm Model

In COMSOL Multiphysics, the two-dimensional axisymmetric plasma bar-plate corona discharge model is used for modeling and simulation. The model is solved by the plasma module of COMSOL Multiphysics software. The geometric structure is shown in Figure 1. The curvature radius of the rod electrode is 0.2 mm. The gap distance between the rod and plate is 5.5 mm. The solution domain width is 5 mm. The applied voltage is -1 kV. The computing time is 300 ns, and the step is 1 ns. The corona discharge belongs to a low-temperature discharge. The gas temperature is 293 K.

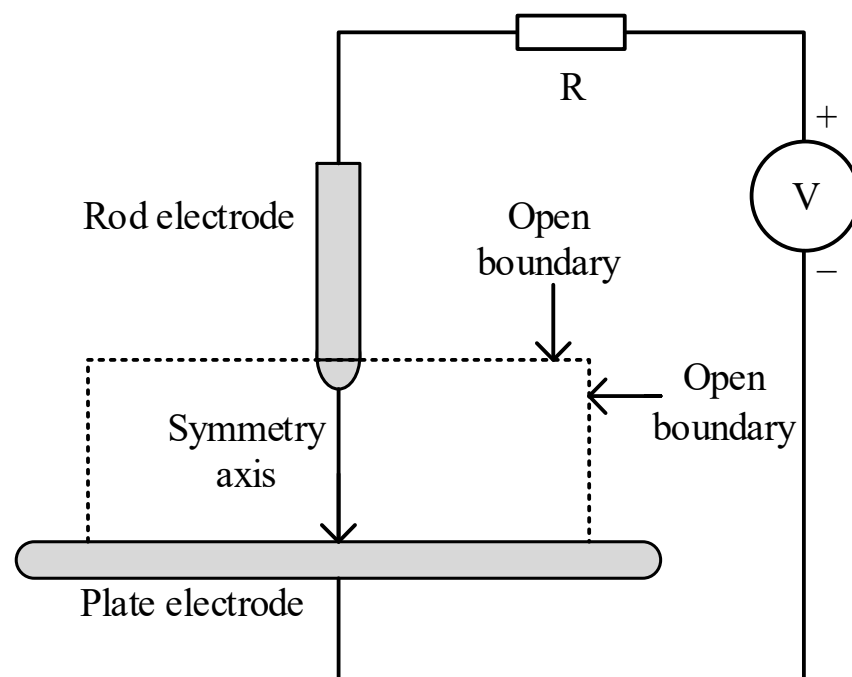


Figure 1. Geometric structure diagram of bar-plate model.

The meshing of the computational domain in the simulation is shown in Figure 2. Refinements are made at the reaction tip and in the region below, making the mesh very dense. In other areas with the weak responses, it does not need to be too dense, which can ensure accurate results and save calculation time.

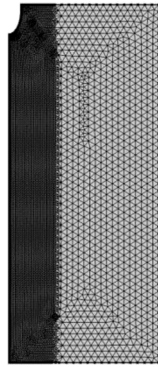


Figure 2. Meshing of the computational domain.

In electron transport theory, the definition of boundary conditions is helpful for the convergence and accuracy of the results. Determining the appropriate boundary conditions according to the physical environment is essential when solving partial differential equations. Secondary electron emission is an important mechanism to maintain the further development of negative corona discharge. For corona discharge, especially negative corona discharge, the cathode boundary condition must consider the emission process of secondary electrons.

The specific boundary conditions are set as follows [21,22]:

Given the secondary emission process, the electrons move several times on the wall with average free travel, then dissipate, and the boundary conditions causing electron flux are expressed as:

$$n \cdot \Gamma_e = \left(\frac{1}{2} v_{e,th} n_e \right) - \sum_i \gamma_i (\Gamma_i \cdot n) \quad (6)$$

The boundary conditions of electron energy flux at positive and negative electrodes are expressed as follows:

$$n \cdot \Gamma_\varepsilon = \left(\frac{5}{6} v_{e,th} n_\varepsilon \right) - \sum_i \gamma_i \varepsilon_i (\Gamma_i \cdot n) \quad (7)$$

where Γ_i is the ion density flux, $1/(\text{m}^2 \cdot \text{s})$. $v_{e,th}$ is the electron thermal rate, $v_{e,th} = \sqrt{8k_B T_e / \pi m_e}$, m/s. k_B is the Boltzmann constant, J/K. m_e is the electronic mass, kg. γ_i is the secondary electron emission coefficient caused by positive ion collision with cathode. ε_i is the average energy of the secondary electron.

For heavy particle substances, ions will be lost on the wall under the action of surface reactions, and the electric field will point directly to the wall.

The boundary conditions of positive and negative ions are expressed as follows:

$$n \cdot \Gamma_i = \frac{1}{4} v_{i,th} n_i + \alpha n_i \mu_i E \cdot n \quad (8)$$

where

$$v_{i,th} = \sqrt{8k_B T / \pi m_i} \quad (9)$$

$$\alpha = \begin{cases} 1 & \mu_i E \cdot n > 0 \\ 0 & \mu_i E \cdot n \leq 0 \end{cases} \quad (10)$$

The second term of Equation (8) can be simplified by the boundary conditions of neutral particle flux at the positive and negative electrodes, that is,

$$n \cdot \Gamma_i = \frac{1}{4} v_{i,th} n_i \quad (11)$$

where $v_{i,th}$ is the ion movement rate, m/s. T is the particle temperature, K. m_i is the mass of ions, kg. n_i is the ion number density, $1/m^3$. μ_i is the ion migration rate, $m^2/(V \cdot s)$.

The density flux satisfied by all particles under open boundary conditions is

$$n \cdot \nabla n_k = 0 \quad (12)$$

The boundary condition satisfied by the potential is expressed as follows:

$$n \cdot \nabla \varphi = 0 \quad (13)$$

3. Air Negative Corona Discharge Morphology Analysis

The charge in the bar-plate gap moves directionally from a current due to the action of a strong field. According to the current calculation equation obtained from Sato's research [23], the current is presented as follows:

$$I = \frac{e}{V_0} \iint 2\pi r (\mu_p n_p + \mu_e n_e + \mu_n n_n) \vec{E} \cdot \vec{E}_L dr dz \quad (14)$$

where V_0 is the applied voltage, V; \vec{E}_L is the Laplace electric field, V/m; and μ_p , μ_n , and μ_e are the positive ion, negative ion, and electron mobility, $m^2/(V \cdot s)$, respectively.

Through model construction and parameter setting, we can study the model. Based on the calculation of air corona discharge, the transient characteristics of plasma are studied in this model. After typing the time step, the system begins solving. Figure 3 shows the typical negative corona discharge current calculated by this model. The current waveform curve has five main stages: discharge starting time (t_1), current rising stage (t_1-t_2), current falling stage (t_2-t_3), current stabilizing stage (t_3-t_4), and current stabilizing stage (t_4-t_5). The current in the discharge starting stage is tiny (approximately $8 \mu A$), and the current increases rapidly to 1.934 mA in t_1-t_2 . In t_2-t_3 , the current decrease slowly, the current in t_3-t_4 gradually tends to be stable, and the current remains approximately $10.5 \mu A$ stably in t_4-t_5 .

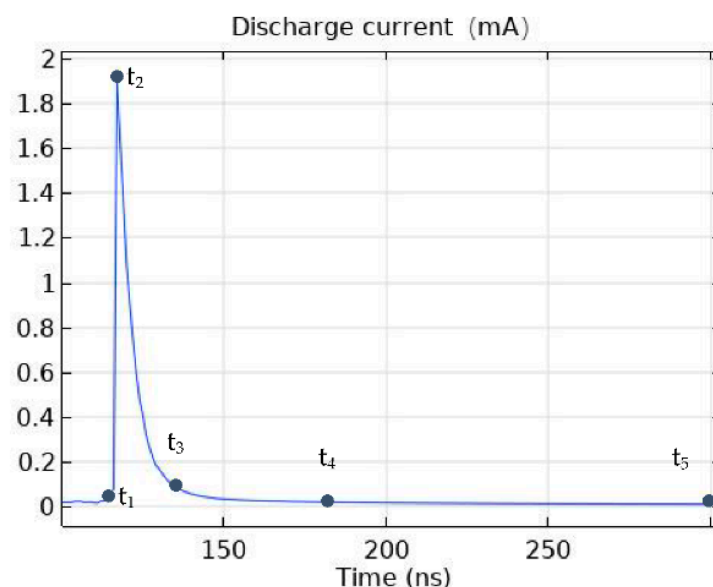


Figure 3. Negative corona discharge current waveform.

Figure 4 shows the electric field intensity E , space charge density ρ , electron number density N_e , positive ion density N_p (N_2^+ , N_4^+ , O_4^+ , O_2^+ , and $N_2O_2^+$), and negative ion density N_n (O_2^- and O^-) at different times of each stage.

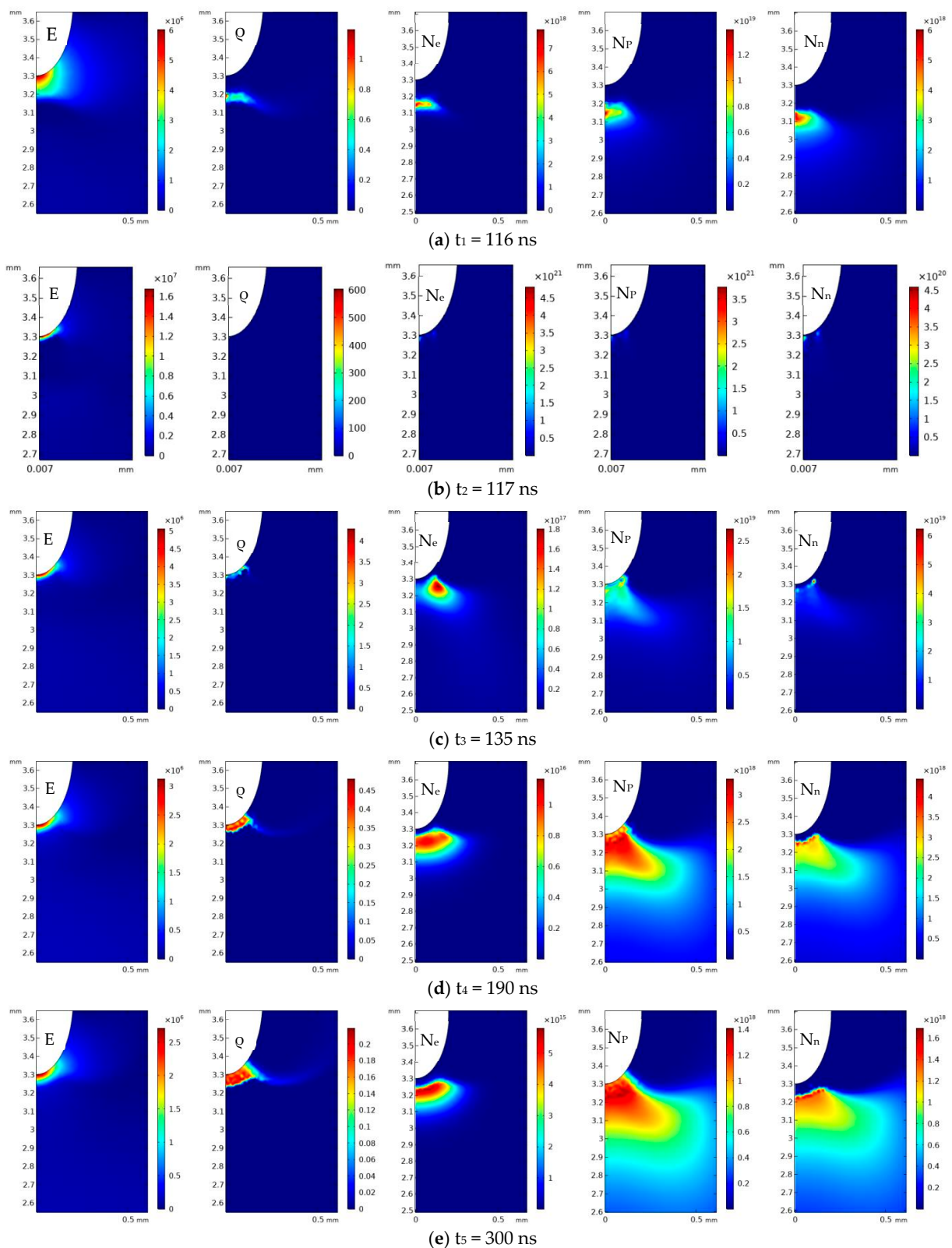


Figure 4. Corona discharge morphology at different times.

In the early stages of corona discharge development ($t = 116$ ns), the maximum rod field strength is 60 kV/cm, which is greater than the initial breakdown field strength of the air negative bar-plate gap. Next, the air ionizes positive ions and electrons rapidly under the action of an applied electric field, and the number density of positive ions and

electrons in the gap increases gradually. The positive ions on the surface of the plate move to the rod, collide with the rod electrode, produce secondary electrons, and quickly form an electron avalanche. Due to the adsorption, some electrons are adsorbed by neutral molecules in the air to form negative ions. The negative ions and electrons migrate to the plate electrode under the action of electric field force. The electrons continue to adsorb to form negative ions in the process of migration, making the number of negative ions gradually increase. At 116 ns, the maximum number density of electrons is $7.8 \times 10^{18} \text{ m}^{-3}$, the positive and negative ions reach $1.4 \times 10^{19} \text{ m}^{-3}$ and $6.0 \times 10^{18} \text{ m}^{-3}$, and the space charge density reaches 1.2 C/m^3 .

With the development of discharge, the space electric field is distorted, and the air continues to ionize under the action of the distorted electric field. The number density of positive ions increases continuously, and the number of negative ions produced by electron adsorption also accumulates rapidly. Then the space charge density increases rapidly.

In the bar-plate gap, positive ions constantly move toward the rod electrode, electrons and negative ions move toward the plate electrode, forming a discharge current. The current value increases with the increase in electron and ion number density and reaches a peak of 1.934 mA at 117 ns. At this time, the number density of electrons, positive and negative ions reach the maximum values, which are $4.8 \times 10^{21} \text{ m}^{-3}$, $3.8 \times 10^{21} \text{ m}^{-3}$, and $5.5 \times 10^{20} \text{ m}^{-3}$. The maximum space charge density increases to 605 C/m^3 . Then, the discharge enters the next stage.

In the current drop stage ($t = 117\text{--}135 \text{ ns}$), some positive ions react with negative ions to gradually reduce the number of positive and negative ions. At the same time, negative ions and electron clusters diffuse to the plate electrode to form a large diffusion radius (Figure 4c). In the bar-plate gap, the original electric field intensity is weakened, the ionization rate is also reduced, and the electron number density and positive ion number density decrease accordingly. The weakened electron adsorption reduces the negative ion number density. When $t = 135 \text{ ns}$, the number density of electron, positive ion, and negative ion are reduced to $1.8 \times 10^{17} \text{ m}^{-3}$, $2.7 \times 10^{19} \text{ m}^{-3}$, and $6.3 \times 10^{19} \text{ m}^{-3}$, and the space charge density decreases to 4.3 C/m^3 .

After that, the charge density becomes too low to distort the electric field. As a result, the electric field intensity decreases, and the electron production rate decreases. In the period of $t = 190 \text{ ns}$ to 300 ns , the electron number density decreases from $1.1 \times 10^{16} \text{ m}^{-3}$ to $5.8 \times 10^{15} \text{ m}^{-3}$, and the electron avalanche tends to end gradually. The number of positive and negative ions decreases and tends to be stable. The maximum number density of positive ions reduced from $3.3 \times 10^{18} \text{ m}^{-3}$ to $1.4 \times 10^{18} \text{ m}^{-3}$, and the negative ion declined from $4.4 \times 10^{18} \text{ m}^{-3}$ to $1.7 \times 10^{18} \text{ m}^{-3}$. The ion movement in the gap decreases, and the discharge current tends to be stable.

4. Research on Plasma Chemical Reaction

4.1. Importance Analysis of Chemical Reactions

This model has identified 23 plasma chemical reactions based on previous studies. Since the rate of collision reaction can reflect the intensity of the reaction process in air discharge [7], the reaction rates of plasma chemical reactions involved in different discharge periods are studied in this paper, and the plasma reactions that played a major role in several typical moments are obtained, as shown in Figure 5.

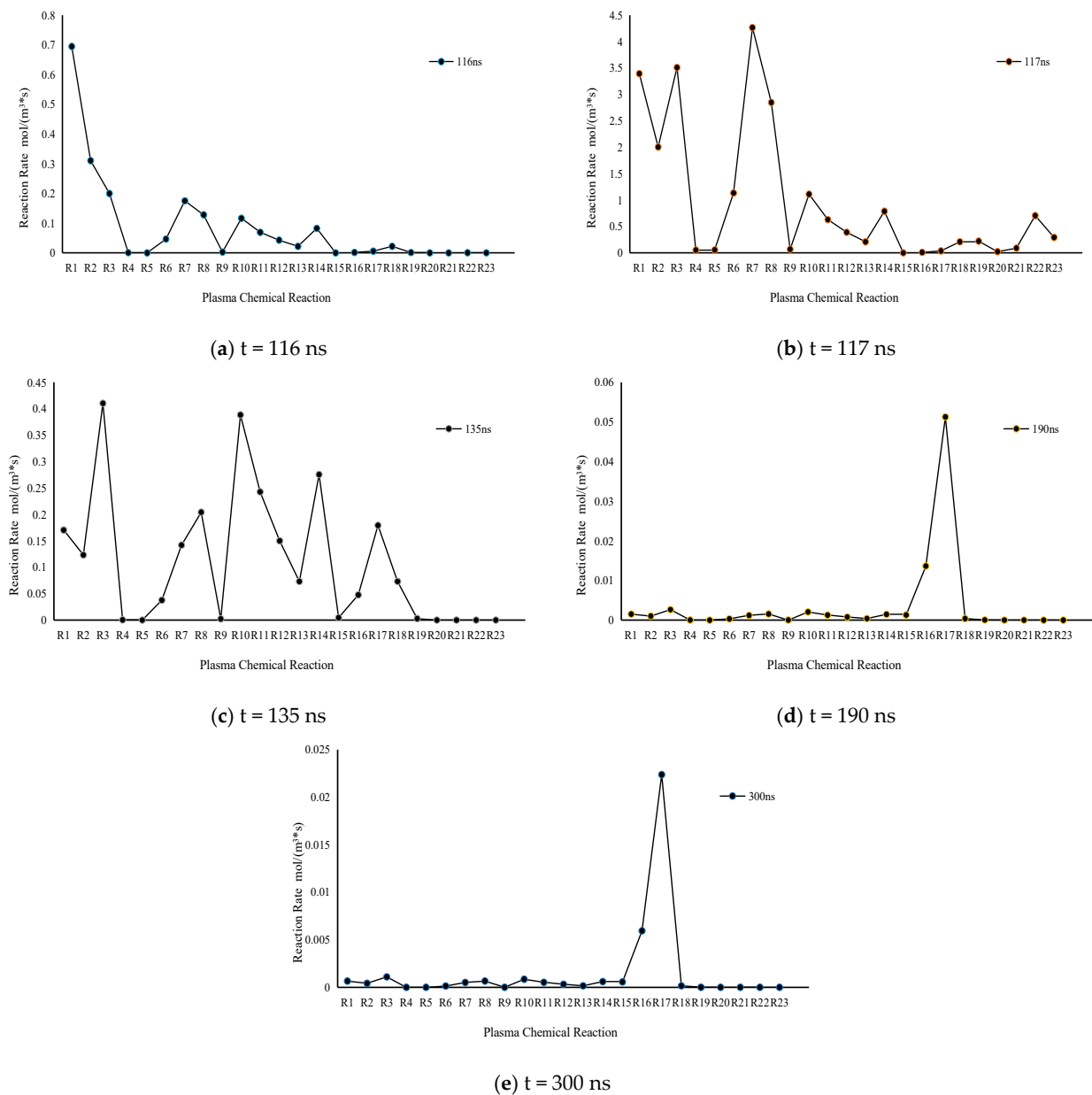


Figure 5. Reaction rate at five typical times.

Collision ionization reactions, electron adsorption reactions, charge transfer reactions, and composite reactions are considered in the micro process of the corona discharge. The maximum reaction rate is used to characterize the importance of the reaction in the discharge process. We can see from Figure 5a that the first three major reactions at the initial stage of the discharge are R₁, R₂, and R₃, namely collision ionization and electron adsorption reactions. At this stage, positive ions and electrons are generated by gas collision ionization, and electrons are absorbed by neutral molecules to form negative ions. The number of charged particles begins to increase.

As shown in Figure 5b, when $t = 117$ ns, except for collision ionization reactions (e.g., R₁, R₂) and electron adsorption reaction (e.g., R₃), the charge transfer reactions (e.g., R₇ and R₈) begin to play a role, generating a large amount of O₂⁺. At this time, the rates of all reactions reach the maximum, the reactions are the most intense, and the number of charged particles reaches a peak.

In Figure 5c, when $t = 135$ ns, the rates of all reactions decrease. At this time, the major reactions are the electron adsorption reaction (e.g., R_3) and part of the charge transfer reactions (e.g., R_8 , R_{10} , R_{11} , and R_{14}), and the number of positive and negative ions decreases. Meanwhile, the rate of composite reactions (e.g., R_{16} , R_{17} , and R_{18}) begins to increase gradually, resulting in declining charged particles in the gap and the end of the electron avalanche.

As shown in Figure 5d,e, during $t = 190$ – 300 ns, the main chemical reactions are composite reactions (e.g., R_{16} and R_{17}). The reaction rates of the rest of the plasma are close to zero, indicating that the generation reaction of charged particles is basically over in this period. In the gap, the positive ion O_4^+ and the negative ion O_2^- react and combine to generate the neutral particle O_2 . The reaction becomes weaker and weaker, marking the end of the corona discharge.

Based on the above analysis, the primary plasma chemical reactions at each typical time are obtained according to the change in reaction rate, and the corresponding discharge current and changes in microparticles are further formed.

4.2. Distribution of Heavy Particles

To further study the discharge characteristics of air at DC voltage, the distribution characteristics of heavy particles at different discharge periods are discussed in this model, which is taken as a factor to describe the micro process of air discharge at the DC negative polarity bar-plate gap. The values and corresponding curves of the maximum number density of the spatial distribution of heavy particles at different times are shown in Table 3 and Figure 6.

Table 3. The number density of heavy particles at different times.

Particle	Maximum Number Density of Heavy Particles/ m^{-3}				
	116 ns	117 ns	135 ns	190 ns	300 ns
O_2^+	5.7×10^{18}	1.5×10^{21}	8.8×10^{17}	4.0×10^{16}	1.5×10^{16}
O_4^+	5.9×10^{18}	1.8×10^{20}	2.6×10^{19}	3.3×10^{18}	1.4×10^{18}
N_2^+	3.3×10^{18}	1.1×10^{21}	8.3×10^{16}	5.1×10^{15}	1.9×10^{15}
N_4^+	2.0×10^{18}	1.2×10^{21}	1.8×10^{17}	9.5×10^{15}	3.5×10^{15}
$N_2O_2^+$	1.5×10^{17}	4.2×10^{19}	2.3×10^{16}	1.0×10^{15}	3.9×10^{14}
O^-	6.1×10^8	6.2×10^8	4.7×10^{10}	1.5×10^{10}	5.3×10^9
O_2^-	6.0×10^{18}	4.6×10^{20}	6.2×10^{19}	4.4×10^{18}	1.7×10^{18}
O	6.8×10^{11}	1.1×10^{17}	8.9×10^8	4.2×10^6	1.6×10^6
O_3	5.3×10^{17}	2.0×10^{21}	8.4×10^{21}	7.0×10^{21}	4.9×10^{21}

According to Table 3 and Figure 6, the number density of positive ions in the discharge process mainly depends on O_2^+ and O_4^+ , and the number of positive ions that contain N is relatively small. This is because, on the one hand, N_2^+ and O_2^+ mainly come from the collision ionization of N_2 , O_2 , and e. The collision ionization energy loss of O_2 is 12.1 eV, and the collision ionization energy loss of N_2 is 15.6 eV. Collision ionization of O_2 is relatively easy to occur. On the other hand, in the charge transfer reaction equations, N-containing ions are prone to charge transfer reaction to generate O-containing positive ions, and the reaction rate is fast, whereas O_4^+ can be generated from O_2^+ through the charge transfer reaction. Therefore, the number density of positive ions that contain O is higher than that of positive ions that contain N.

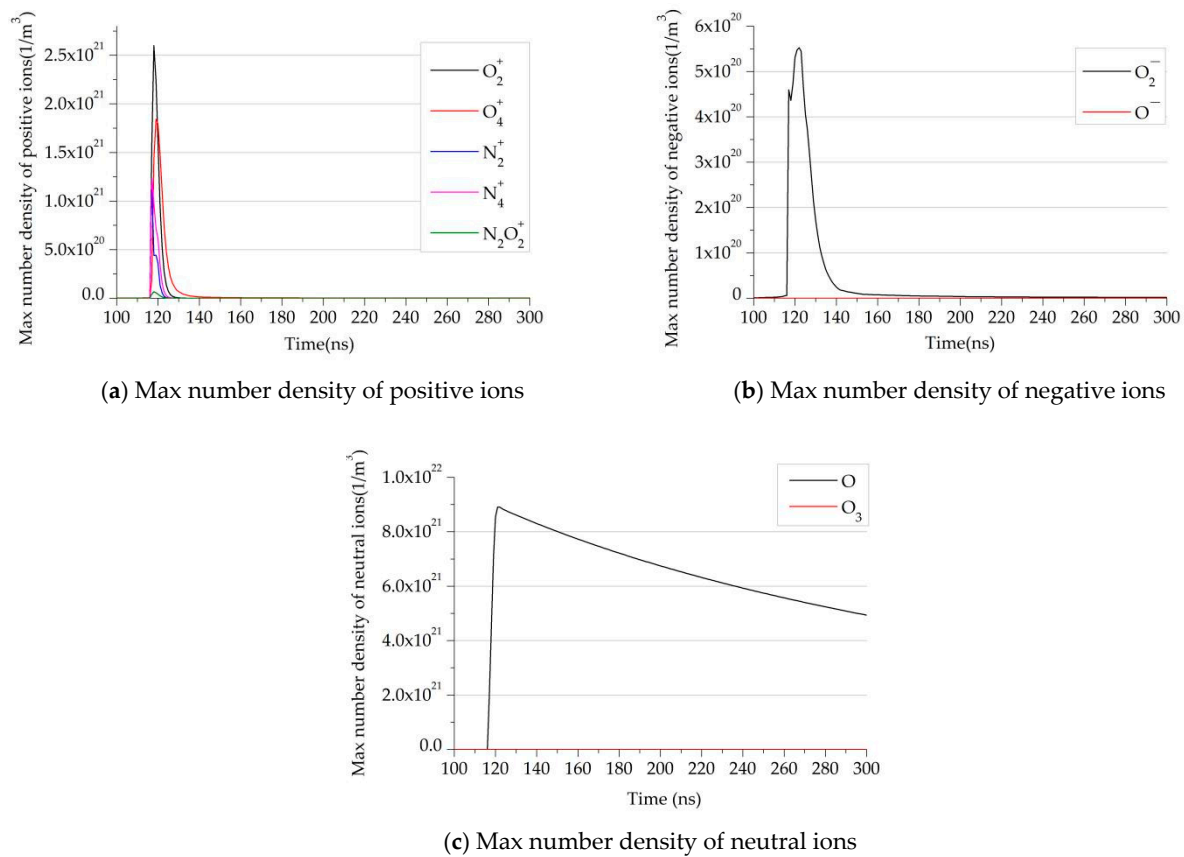


Figure 6. The maximum number density distribution of heavy particles.

The number density of negative ions is mainly determined by O_2^- , which is generated by the adsorption reaction of O_2 adsorbed free electrons. The number density of negative ions is lower than that of positive ions. The reason is that neutral particles are difficult to absorb fast-moving electrons, and the O_2^- generated will react with O_2^+ or O_4^+ to form neutral molecules. In corona discharge, collision ionization is dominant, which leads to a lower number density of negative ions. Neutral particles are mainly O, except N_2 and O_2 . Neutral particles have minimal effects on the ionization reaction, and their role in corona discharge reaction does not need to be considered too much.

5. Conclusions

In this paper, the characteristics of negative corona discharge in the bar-plate gap are simulated, and the main conclusions are presented as follows:

- (1) A negative corona discharge model based on the plasma discharge model, in which collision ionization reaction, charge transfer reaction, recombination reaction, electron adsorption reaction, and surface reaction are considered, is proposed.
- (2) When the rod applied voltage is -1 kV, the discharge current curve shows a pulse change trend. Within a discharge pulse cycle, the curve can be divided into the current rising stage, the current falling stage, the current tending to stable stage, and the current stable stage. At the same time, the distribution morphology of particles at different stages of corona discharge is obtained, which is highly consistent with the literature results.
- (3) In the process of negative corona discharge, the maximum reaction rate indicates the importance of plasma reaction at each stage. The collision ionization reactions (e.g., R_1 and R_2) and electron adsorption reaction (e.g., R_3) play a primary role in the current rising period, resulting in an increase in charged particles and the formation of an electron avalanche. In the current drop phase, all reaction rates decreased. Except for

collision ionization and electron attachment, partial charge transfer reactions (e.g., R_8 , R_{10} , R_{11} , and R_{14}) and composite reactions (e.g., R_{16} , R_{17} , and R_{18}) begin to play their role, making the number of charged ions in the gap gradually decrease. Composite reactions (e.g., R_{16} and R_{17}) are mainly present in the current stabilization stage, and the other reaction rates are almost zero. The corona discharge is over.

- (4) Among all the particles involved in the plasma reactions, the positive ion number density of O_2^+ and O_4^+ accounts for the most significant proportion of all positive ions, and the negative ion O_2^- is the most abundant particle. The neutral particle is mainly O except for N_2 and O_2 . The neutral particles have little influence on the ionization reaction and corona discharge.

Author Contributions: Conceptualization, N.F. and T.M.; methodology, N.F. and C.C.; software, N.F.; validation, N.F., B.Y. and W.G.; formal analysis, B.Y.; investigation, W.G.; resources, C.C.; writing—original draft preparation, N.F.; writing—review and editing, N.F., T.M. and C.C.; supervision, T.M.; project administration, C.C.; funding acquisition, C.C. All authors have read and agreed to the published version of the manuscript.

Funding: This research was funded by Young Academic Leader of North University of China, grant number QX202002.

Institutional Review Board Statement: Not applicable.

Informed Consent Statement: Not applicable.

Data Availability Statement: Not applicable.

Conflicts of Interest: The authors declare no conflict of interest.

References

- Sun, J.; Sun, L.; Chen, W.; Li, Z.; Yan, X.; Xu, Y. Metal particle movement and distribution characteristics under AC voltage and ball-plane electrodes. *High Volt.* **2019**, *4*, 138–143. [\[CrossRef\]](#)
- Xu, P.; Zhang, B.; He, J.; Chen, S. Influence of humidity on the characteristics of negative corona discharge in air. *Phys. Plasmas* **2015**, *22*, 093514. [\[CrossRef\]](#)
- Xu, P.; Zhang, B.; Chen, S.; He, J. Influence of humidity on the characteristics of positive corona discharge in air. *Phys. Plasmas* **2016**, *23*, 063511. [\[CrossRef\]](#)
- Kokovin, A.O.; Kozyrev, A.V.; Kozhevnikov, V.Y. Simulation of negative corona discharge in atmospheric air: From mode of Trichel pulses to stationary discharge. *J. Phys. Conf. Ser.* **2021**, *2064*, 12024. [\[CrossRef\]](#)
- Fofana, I.; Beroual, A. A model for long air gap discharge using an equivalent electrical network. *IEEE Trans. Dielectr. Electr. Insul.* **1996**, *3*, 273–282. [\[CrossRef\]](#)
- Liang, H.; Du, B.; Li, J.; Du, Q. Numerical simulation on the surface charge accumulation process of epoxy insulator under needle-plane corona discharge in air. *IET Sci. Meas. Technol.* **2017**, *12*, 9–16. [\[CrossRef\]](#)
- Liu, K.; Liao, R.; Zhao, X. Numerical simulation of the characteristics of electrons in bar-plate dc negative corona discharge based on a plasma chemical model. *J. Electr. Eng. Technol.* **2015**, *10*, 1804–1814. [\[CrossRef\]](#)
- Ayubi, B.I.; Zhang, L.; Sun, Y.; Qi, Y.Y. Fluid-Kinetic Model for Numerical Simulation of Gas-Solid Insulation Surface Discharge. In Proceedings of the SCEMS 2020-3rd Student Conference on Electric Machines and Systems (SCEMS 2020), Jinan, China, 4–6 December 2020. [\[CrossRef\]](#)
- Chen, S.; Nobelen, J.C.P.Y.; Nijdam, S. A self-consistent model of ionic wind generation by negative corona discharges in air with experimental validation. *Plasma Sour. Sci. Technol.* **2017**, *26*, 095005. [\[CrossRef\]](#)
- Gao, Q.; Niu, C.; Adamiak, K.; Rong, M.; Wang, X. Numerical simulation of negative point-plane corona discharge mechanism in SF_6 gas. *Plasma Sour. Sci. Technol.* **2018**, *27*, 115001. [\[CrossRef\]](#)
- Wu, F.; Liao, R.; Wang, K.; Yang, L.; Grzybowski, S. Numerical Simulation of the Characteristics of Heavy Particles in Bar-Plate DC Positive Corona Discharge Based on a Hybrid Model. *IEEE Trans. Plasma Sci.* **2014**, *42*, 868–878. [\[CrossRef\]](#)
- Peng, Y.; Chen, X.; Deng, Y.; Lei, L.; Haoyu, Z.; Pei, X.; Chen, J.; Yuan, Y.; Wen, X. Kinetic study of key species and reactions of atmospheric pressure pulsed corona discharge in humid air. *Plasma Sci. Technol.* **2022**, *24*, 055404. [\[CrossRef\]](#)
- Liao, R.J.; Wu, F.F.; Yang, L.J.; Wang, K.; Zhou, Z.; Liu, K.L. Investigation on microcosmic characteristics of Trichel pulse in bar-plate DC negative corona discharge based on a novel simulation model. *Int. Rev. Electr. Eng.* **2013**, *8*, 504–512.
- He, Y.; Sun, A.; Xue, J.; Shen, Z.; Zhang, X.; Zhang, G. Experimental study on pulse characteristics of negative corona discharge in SF_6/N_2 gas mixtures under DC voltages. *AIP Adv.* **2020**, *10*, 055027. [\[CrossRef\]](#)
- Sima, W.; Peng, Q.; Yang, Q.; Yuan, T.; Shi, J. Study of the characteristics of a streamer discharge in air based on a plasma chemical model. *IEEE Trans. Dielectr. Electr. Insul.* **2021**, *19*, 2. [\[CrossRef\]](#)

16. Gazeli, O.; Lazarou, C.; Niu, G.; Anastassiou, C.; Georghiou, G.; Franzke, J. Propagation dynamics of a helium micro-tube plasma: Experiments and numerical modeling. *Spectrochim. Acta Part B At. Spectrosc.* **2021**, *7*, 106248. [[CrossRef](#)]
17. Wang, J.; Guo, R.; Ping, A.; Liu, T.; Han, S.; Li, Q. Research on numerical simulation for partial discharge of epoxy interface excited by high-frequency sinusoidal voltage. *High Volt.* **2021**, *7*, 439–451. [[CrossRef](#)]
18. Nikonov, V.; Bartnikas, R.; Wertheimer, M.R. Surface charge and photoionization effects in short air gaps undergoing discharges at atmospheric pressure. *J. Phys. D Appl. Phys.* **2001**, *34*, 2979. [[CrossRef](#)]
19. Mahadevan, S.; Raja, L. Simulations of direct-current air glow discharge at pressures 1Torr: Discharge model validation. *J. Appl. Phys.* **2010**, *107*, 093304. [[CrossRef](#)]
20. Plasma Data Exchange Project. Available online: <https://fr.lxcat.net> (accessed on 10 November 2021).
21. Farouk, T.; Farouk, B.; Staack, D.; Gutsol, A.; Fridman, A. Simulation of dc atmospheric pressure argon micro glow-discharge. *Plasma Sour. Sci. Technol.* **2006**, *15*, 676–688. [[CrossRef](#)]
22. Tran, T.N.; Golosnoy, I.O.; Lewin, P.L.; Georghiou, G. Numerical modelling of negative discharges in air with experimental validation. *J. Phys. D Appl. Phys.* **2010**, *44*, 15203. [[CrossRef](#)]
23. Morrow, R.; Sato, N. Discharge current induced by the motion of charged particles in time-dependent electric fields; Sato's equation extended. *J. Phys. D Appl. Phys.* **1999**, *32*, L20. [[CrossRef](#)]